11-20-2017

U–Pb Dating of Cave Spar: A New Shallow Crust Landscape Evolution Tool

D. D. Decker
University of New Mexico

V. J. Ployak
University of New Mexico

Y. Asmeron
University of New Mexico

Matthew Lachniet
University of Nevada, Las Vegas, matthew.lachniet@unlv.edu

Repository Citation

Decker, D. D., Ployak, V. J., Asmeron, Y., Lachniet, M. (2017). U–Pb Dating of Cave Spar: A New Shallow Crust Landscape Evolution Tool. *Tectonics, 37*(1), 208-223.
http://dx.doi.org/10.1002/2017TC004675

AGU PUBLICATIONS

Tectonics

RESEARCH ARTICLE
10.1002/2017TC004675

Key Points:
- Not all landscapes contain abundant apatite for (U/Th)-He or fission track thermochronometry
- The depth and age of "cave spar" can be determined through a variety of methods
- In regions where carbonates dominate, cave spar ages can be used in tectonic studies

Correspondence to:
D. D. Decker,
dave.decker@caves.org;
ddecke67@unm.edu

Citation:
Decker, D. D., Polyak, V. J., Asmerom, Y., & Lachniet, M. S. (2018). U–Pb dating of cave spar: A new shallow crust landscape evolution tool. *Tectonics*, *37*, 208–223. https://doi.org/10.1002/2017TC004675

Received 24 MAY 2017
Accepted 7 NOV 2017
Accepted article online 20 NOV 2017
Published online 19 JAN 2018

U–Pb Dating of Cave Spar: A New Shallow Crust Landscape Evolution Tool

D. D. Decker[1], V. J. Polyak[1], Y. Asmerom[1], and M. S. Lachniet[2]

[1]Department of Earth and Planetary Sciences, University of New Mexico, Albuquerque, NM, USA, [2]Department of Geoscience, University of Nevada, Las Vegas, Las Vegas, NV, USA

Abstract In carbonate terranes, rocks types that provide apatite are not available to effectively use apatite fission track (AFT) or (U/Th)-He chronometry (AHe). Here we suggest that calcite cave spar can be an effective chronometer and complimentary to AFT and AHe thermochronometers in carbonate regions such as our study area, the Guadalupe Mountains of southeastern New Mexico, and west Texas. Our measured depth of cave spar deposition is 500 ± 250 m beneath the regional water table, formed at temperatures of 40° to 80°C, indicating that these caves and their spar crystals form near the supercritical CO_2-subcritical CO_2 boundary where we interpret the origin of both the caves and spar to occur. This depth-temperature relationship suggests a higher than normal geotherm, likely associated with regional magmatic activity. As a case study we examined the timing of uplift of the Guadalupe Mountains previously attributed to the compressional Laramide orogeny (ca. 90 to 50 Ma), later extensional tectonics associated with Basin and Range (ca. 36 to 28 Ma) or the opening of the Rio Grande Rift (ca. 20 Ma to Present). We show that most of the spar origin is coeval with the ignimbrite flare-up between 36 and 28 Ma. Our results constrain the initiation of Guadalupe Mountains block uplift, relative to the surrounding terrain, to between 27 and 16 Ma and reconstruct the evolution of a low-lying regional landscape prior to block uplift from 185 to 28 Ma, in support of models that attribute regional surface uplift to extensional tectonics and associated volcanism.

Plain Language Summary A new way of determining the timing of uplift related to mountain building using calcite crystals that grow in deep seated caves is discussed. The calcite crystals and the caves that contain them are the result of high levels of carbon dioxide that is released from magma deep below. These crystals form at a depth determined by the temperature and pressure related to the transition between super-critical carbon dioxide (a state of matter that is neither solid, liquid, nor gas) and gaseous carbon dioxide, usually between 250 and 750 m beneath the water table. For the first time on these types of crystals, we use uranium-lead dating techniques to find the age of these calcite crystals to determine when the crystals formed. We also use microscopic fluid inclusions within the crystals to find the temperatures at which they formed. With these three pieces of information, depth, age, and temperature, we can calculate when the crystals were at a certain depth beneath the water table and the geothermal environment in which they grew, providing a novel way to determine when the mountains may have been uplifted to their present elevation.

1. Introduction

1.1. Background

Two shallow crust (<3 km) thermochronometric methods, apatite fission track (Donelick, O'Sullivan, & Ketcham, 2005; Reiners, Ehlers, & Zeitler, 2005) and apatite (U-Th)/He or AHe thermochronometry, are currently commonly used in shallow landscape evolution studies (Ehlers & Farley, 2003; Farley, 2002; Farley & Stockli, 2002). There are a number of geologic settings in which these techniques are not useable due to lack of the rocks that contain the minerals used in these methods (Donelick et al., 2005). Moreover, these techniques have led to some disparate conclusions regarding interpretations of shallow depth data (Donelick et al., 2005; Flowers & Farley, 2012, 2013; Green et al., 2006; Hendricks & Redfield, 2005, 2006; Karlstrom et al., 2013, 2014; Larson et al., 2006). In this study we show that large calcite crystals, herein referred to as cave spar (druses of euhedral calcite crystals 2–30 cm in length, lining small geode-like caves, Figure 1a), can be used as an effective depth and time indicator for landscape evolution studies, complimentary to the apatite fission track and apatite (U/Th)-He thermochronometers for use in landscape evolution studies (Decker, Polyak, & Asmerom, 2015). This method is not based on the temperature at which fission tracks heal themselves, or

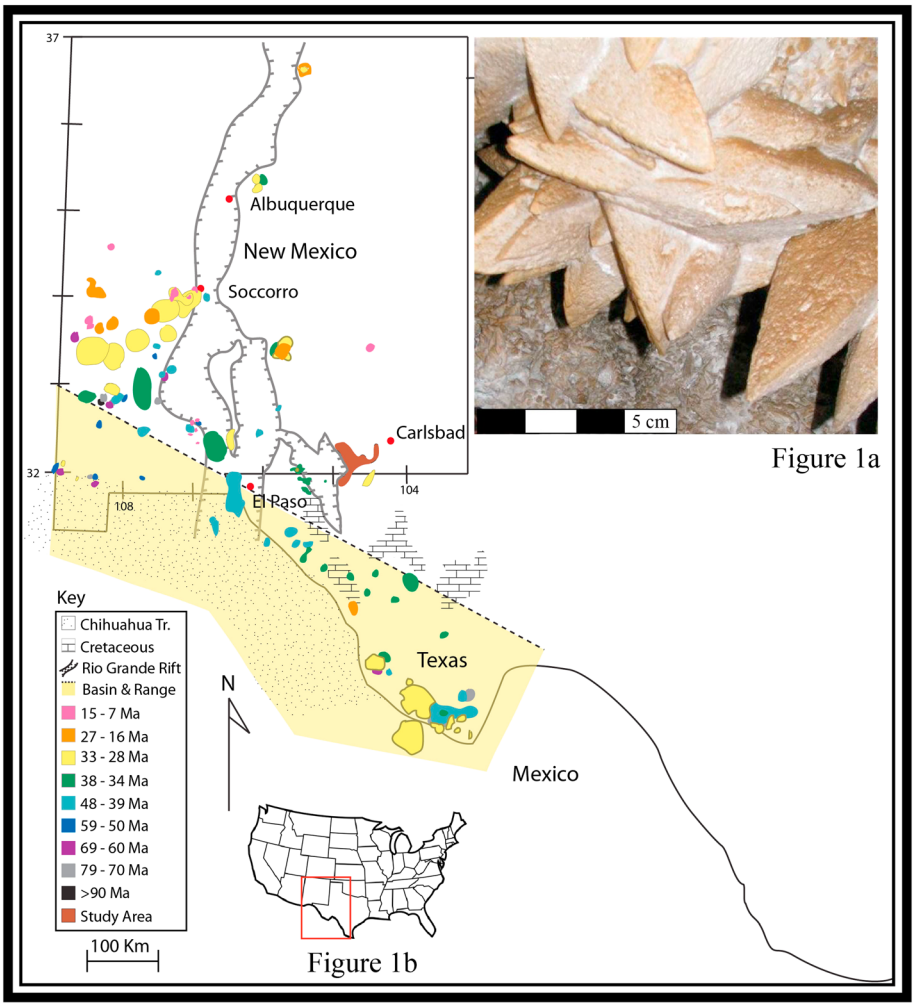

Figure 1. (a) Representative spar cave from CAVE-005 in Carlsbad Caverns National Park. The spar cave lined with euhedral calcite spar is approximately 30 m in the long axis, and the walls, floor, and ceiling are entirely covered in euhedral spar up to 30 cm in length. (b) Overview of the Guadalupe Mountains of southeastern New Mexico and Trans-Pecos Texas. Here we show the known periods of magmatism in physical relation to our study area.

the amount of gaseous daughter nuclides accumulated in the crystal structure; rather, we are able to determine the timing of crystal formation with U–Pb isotope ratios (this study), directly measure depth of crystal formation (Decker et al., 2015) based on their ages, and determine their hydrothermal origin using strontium, oxygen, and carbon isotopes. Thus, a single isochron age is coupled to the depth of origin of cave spar crystals, and multiple samples provide multiple ages that correspond to that spar depth. We demonstrate the potential of this new method using the Guadalupe Mountains of southeastern New Mexico and west Texas (Figures 1b and 2), as a proof of concept where our measured U–Pb spar ages are used to constrain the timing of the initiation of the rotation of the Guadalupe Mountains tectonic block (Guadalupe block) as well as the evolution of the landscape prior to block movement relative to the surrounding terrain.

1.2. Cave Spar Model

From depths of formation of three cave spar samples, one from Grand Canyon and two from the Guadalupe Mountains (Decker et al., 2015), we constructed a new cave genesis (speleogenesis) model that explains the origin of these small (<30 m in diameter) geode-like caves (spar caves) and the calcite cave spar that lines them. The three depths show that spar cave speleogenesis and its final phase, cave spar deposition, take place at 500 ± 250 m below a regional water table, which corresponds to the effective pressure (P_e) of the supercritical CO_2-subcritical CO_2 boundary (Decker et al., 2015). We determined a measured depth using a

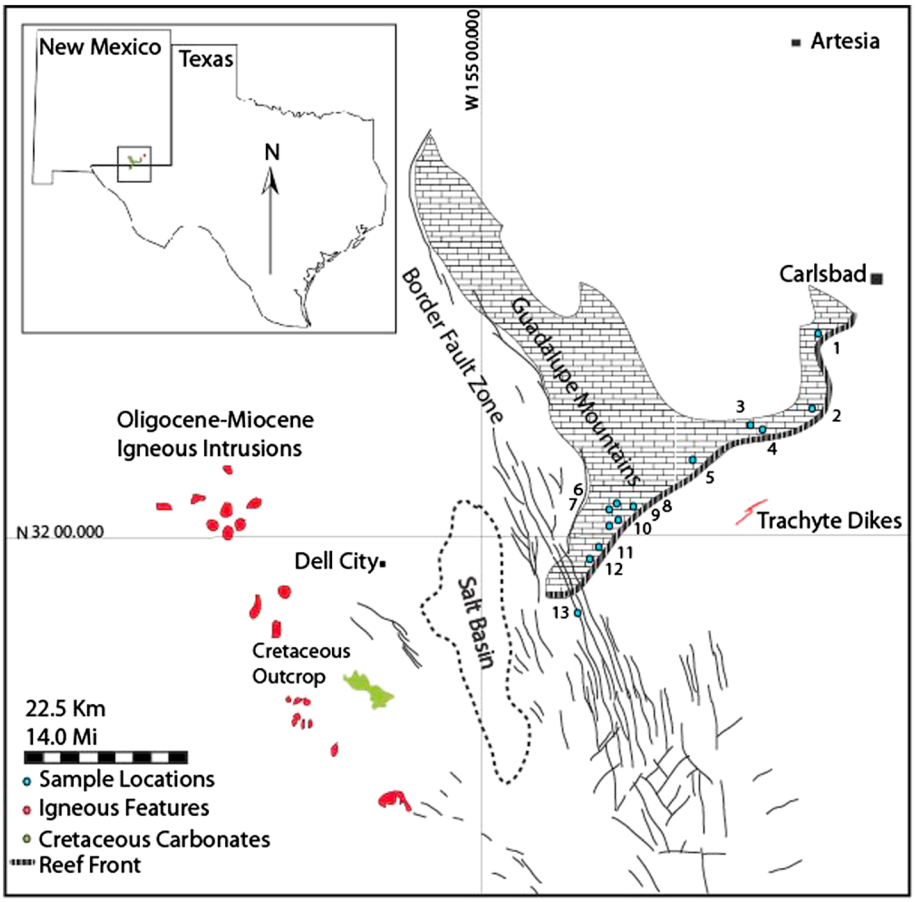

Figure 2. Selected sample locations and nearby igneous features in the Guadalupe Mountains, southeastern New Mexico, and west Texas. 1: BLMC-005; 2: BLMC-002; 3: CAVE-004 and CAVE-006; 4: CAVE-002, CAVE-003, CAVE-007, CAVE-008, and CC-001; 5: CAVE-011; 6: USFS-006; 7: USFS-002 and USFS-007; 8: USFS-008; 9: USFS-009; 10: BLMC-011; 11: GUMO-002 and GUMO-003; 12: GUMO-001; 13: GUPA-001.

Grand Canyon cave spar that formed in the Redwall Limestone 232.3 ± 1.8 Ma (U–Pb age of spar) and, based the measured depth on near-sea level Triassic Moenkopi lithology, positioned 750 m above the cave spar (Decker et al., 2015). The two Guadalupe Mountains spar sample depths were derived by extrapolating the elevation of the water table based on the alunite-age water table position (Polyak et al., 1998) (alunite is formed at/near the water table; therefore, dating the alunite provides the time and elevation of the paleo-water table). In addition to depth of formation of cave spar (Crysdale, 1987; Mruk, 1985), the cave spar temperature of homogenization (T_h) (Crysdale, 1987; Mruk, 1985, 1989) using fluid inclusion assemblage (FIA) analysis of the spar within the spar caves in the Capitan formation and back reef equivalents (cave-forming strata) will yield formation temperatures consistent with those measured by Crysdale (1987) between roughly 50° and 100°C and can be used to determine the hydrostatic pressure at which these minerals formed. These temperatures and pressures are consistent with a supercritical CO_2 speleogenesis model for the spar caves and the calcite cave spar lining them (Decker et al., 2015).

Our model states that during episodes of magmatic activity, CO_2 is released from the magma body in a supercritical state. Since scCO_2 is much less dense and more fluid than the surrounding rock, it makes its way toward the surface relatively easy. In its supercritical state, the CO_2 is not absorbed into water as it rises into an aquifer. At a point roughly 500 m below the water table surface, however, due to decreases in both temperature and pressure, the CO_2 transforms states from supercritical to subcritical and is immediately absorbed into the aquifer where it acidifies the water and consequently dissolves the limestone. This dissolved limestone is carried away by the hydrologic flow and is replaced by more acidic water as long as

the magmatically driven hydrothermal system is active, continuing to dissolve voids at a $scCO_2$-$subCO_2$ horizon. Once the magmatic activity ceases, the waters within the voids become slightly supersaturated and, at the temperatures and pressure at that depth, form the scalenohedral spar of interest. Because we can measure and model the depth (pressure), timing, and temperature of calcite spar formation, our results are used in a similar manner as low-temperature apatite thermochronometers (Chew & Spikings, 2015; Dumitru, 2000; Renne, 2000).

1.3. Regional Geologic History

The Guadalupe Mountains have been heavily studied over the past 70 years; indeed, they are the type location for Permian reef systems. Numerous authors have produced large, in-depth volumes on the geology of the region (Austin, 1978; Flawn, 1956; Garber, Grover, & Harris, 1989; Hayes, 1964; Hayes & Adams, 1962; Hill, 1987, 1996; Kelley, 1971; King, 1948; Kirkland, 2014; Meyer, 1966), and therefore, we will only briefly cover it here. Our area of interest spans from southeastern New Mexico into west Texas and includes the Diablo Plateau, the Guadalupe Mountains, the Delaware Basin, and the Gypsum Plains (Figures 1 and 2). The region is well known for its petroleum production (Permian Basin), potash deposits, large, well-decorated sulfuric acid type caves, and the Waste Isolation Pilot Plant (Hill, 1993). The basement rocks in the region belong to the Texas craton and are mostly granitic. These rocks were emplaced during the Grenville orogeny approximately 1.24 Ga (Flawn, 1955; Wasserburg et al., 1962) and are found approximately 3.3 km below the surface (Flawn, 1956). The Tabosa basin existed in the same location as the Delaware and Midland basins (Hill, 1996) during the Late Proterozoic through the Mississippian and was probably formed by continental rifting in the Proterozoic to Cambrian (Hills, 1984). This basin was dissected by the Central Basin Uplift during the late Mississippian Ouachita orogeny. The entire region remained near sea level during this phase and accumulated vast amounts of sediment (Hill, 1996). During the Permian, the area was inundated by the sea forming a restricted basin where the massive Capitan limestones and Artesia Group back reef sediments were deposited followed by the Castile, Salado, Rustler, and Dewey Lake evaporite formations (Hill, 1987). The area was tectonically quiescent through the remaining Paleozoic and Mesozoic and was not disturbed again until possibly the beginning of the Cenozoic during the initiation of the Laramide orogeny (Eaton, 2008). At some point after the Cretaceous, the region was uplifted from sea level to its current elevation of approximately 2.66 km at its highest point in the Guadalupe Mountains.

There are competing models that describe the timing of the uplift of the Guadalupe block. One model measured 1 km of relative Guadalupe block uplift from 12 Ma to present coeval with Rio Grande rifting (Polyak et al., 1998). Other models suggest that the area arose primarily during the Laramide Orogeny (DuChene & Cunningham, 2006; Eaton, 2008) or during the Oligocene-Miocene (King, 1948). Pre-Laramide crustal thickening has been suggested based on petrographic evidence (Scholle, Ulmer, & Melim, 1992). With the exception of the phase of apparent uplift during Rio Grande rifting, a more robust tectonic history of the Guadalupe Mountains region, in which absolute timing of events is critical, is lacking.

The Guadalupe Mountains spar caves examined in this study are largely confined within the cave-forming strata (Hill, 1996) of the Capitan Limestone and the backreef equivalents of the Yates, Tansil, and Seven Rivers formations. With no known topographic expression for this region before the Guadalupe Mountains tectonic block was uplifted relative to the Salt Basin (Figure 2), our cave spar U–Pb ages are indications of when the cave-forming strata was 500 ± 250 m below a regional water table and likely near this depth below the paleo-surface. Since block uplift and tilting would have moved the cave-forming strata out of the spar forming depths, we can use the thermochronometry and the U–Pb age results from these crystals to reconstruct a deep time history of the Guadalupe Mountains region landscape.

2. Methods

2.1. Sample Selection

Samples were selected from "spar" caves located in the Permian Capitan Reef and immediate backreef and forereef deposits of the Artesia Group (the spar cave-forming strata) along the reef escarpment in the Guadalupe Mountains of New Mexico and Texas (Figure 2). The caves have been described by Decker et al. (2015). The exact cave locations are considered sensitive resource information and can be obtained through the appropriate resource personnel at Carlsbad Caverns National Park, Guadalupe Mountains National Park,

Bureau of Land Management, Carlsbad, and the U.S. Forest Service, Guadalupe District office. Each sample was selected based on its size and lack of visual surface alteration. We collected samples that were already broken or physically damaged to minimize the negative impact to the sampled caves. The samples ranged in size from 4 cm (long axis) to 25 cm. All cave spar samples collected are the mesogenetic spar (formed after the reef stopped growing and before the beginning of H_2SO_4 speleogenesis) described by Hill (1996). Sample location descriptions are available upon request.

2.2. Isotopic Methods

2.2.1. U–Pb Chronology

U–Pb and uranium-series dating methods were used to determine the ages of 22 cave spar crystals, a sample of cave mammillary, and a sample of fault-filling vein calcite. For each spar sample a 1 cm^2 sized piece was extracted from the interior of each spar sample. Surfaces of these pieces were cleaned, placed in clean-room napkins, and broken into smaller subsample pieces. Of these subsamples, 25 to 75 mg pieces were used for the U–Pb geochronology. The high-precision U–Pb, in combination with uranium-series isotope ratios (used to test for open system behavior), was completed using standard isotope dilution anion resin chemistry and mass spectrometry (Denniston et al., 2008; Polyak et al., 1998). Separation of elements was achieved by conventional ion chromatography of spiked samples using Eichrom/Bio-Rad anion exchange resin. A mixed spike containing ^{205}Pb-^{229}Th-^{233}U-^{236}U was used to generate U, Th, and Pb isotope ratios. The U–Pb and uranium-series isotope ratios were measured using the Thermo Neptune Multi-Collector, inductively coupled plasma mass spectrometer (MC-ICP-MS) coupled with the Cetac Aridus II desolvating nebulizer at the University of New Mexico Radiogenic Isotope Lab. U, Th, and Pb aliquots were measured separately. All Pb isotopes were measured using faraday cups with ^{205}Pb (the spike) measured in the center cup using a standard (NBS-981)-sample-sample-standard routine. ^{230}Th and ^{234}U were measured in the center position using the secondary electron multiplier (SEM) or a faraday cup-10^{12}-ohm resistor setup. Gains between the faraday cups and SEM were measured using the NBL-112U standard and an in-house ^{230}Th standard. Decay constants for ^{234}U and ^{230}Th were $2.82206 \pm 0.00302 \times 10^{-6}$ a^{-1} and $9.1705 \pm 0.0138 \times 10^{-6}$ a^{-1}, respectively, from Cheng et al. (2013), and for ^{235}U and ^{238}U were $9.8569 \pm 0.0017/0.0110 \times 10^{-10}$ a^{-1} and $1.54993 \pm 0.00026/0.00219 \times 10^{-10}$ a^{-1}, respectively, from Schoene et al. (2006). Data reduction and isochron ages were calculated using PbDat (Ludwig, 1993) and Isoplot (Ludwig, 2000). One ^{207}Pb-^{206}Pb age was calculated for our oldest sample. Model age routines were written in Excel for the ^{235}U/^{204}Pb-^{207}Pb/^{204}Pb, ^{238}U/^{204}-^{206}Pb/^{204}Pb, and ^{238}U/^{208}Pb-^{206}Pb/^{208}Pb decay systems, using isochron-derived initial ^{235}U/^{207}Pb, ^{238}U/^{204}Pb, and ^{238}U/^{208}Pb ratios and their associated 2σ absolute errors to test for consistency. While these samples are tens of millions of years old, ^{230}Th/^{238}U and δ^{234}U were monitored to test for secular equilibrium and obvious evidence of crystal alteration.

2.2.2. Strontium Isotopes

Subsamples for strontium isotope analyses were 15 to 120 mg powders or pieces. Some pieces were also run for fluid inclusion analyses (see section 2.3.1). The strontium was prepared for isotopic analyses by dissolving each subsample of calcite in 7 N HNO_3, drying the subsample on a hotplate and then preparing a 3 N HNO_3 sample solution for the column resin chemistry. A 2 mL column with 250 μL of Eichrom Sr spec resin was used to retrieve the strontium by chromatographic ion separation with a yield of 81%. Sr spec resin shows no tendency for mass fractionation of ^{87}Sr/^{86}Sr during collection regardless of the amount recovered (De Muynck et al., 2009). Each subsample, dissolved in 3% HNO_3, was then run on the MC-ICP-MS. The standard was NBS-987, which has an ^{87}Sr/^{86}Sr value of 0.71025 (Ma et al., 2013).

2.2.3. Carbon and Oxygen Isotopes

Carbonate samples were reacted at 70°C with three drops of phosphoric acid in a Kiel IV automated carbonate preparation system connected to a Delta V Plus stable isotope ratio mass spectrometer via dual inlet. Isotope values were calibrated to the in-house USC-1 calcite standard, which was calibrated to international calcite standards NBS-18 and NBS-19. Analytical precision is better than 0.08‰ and 0.05‰ for δ^{18}O and δ^{13}C, respectively, based on long-term standard analyses, and values are reported in ‰ notation relative to the VPDB (Vienna Pee Dee Belemnite) scale (Lachniet, 2009).

2.3. Fluid Inclusion Assemblage Methods

2.3.1. Calibration

The fluid inclusion assemblage (FIA) analysis was run on samples for which we had ages using a Leica Leitz Laborlux S microscope equipped with a U.S. Geological Survey modified fluid inclusion heating/cooling

Table 1
U–Pb Ages for 22 Spar Samples, A Cave Mammillary and Vein Filling Calcite

		Concordia		$^{238}U/^{206}Pb$		$^{235}U/^{207}Pb$		$^{207}Pb/^{206}Pb$	
IGSN	Sample #	Age	(Myr)	Age	(Myr)	Age	(Myr)	Age	(Myr)
	97-CAH	91.3	±7.8	(Lundberg et al., 2000)					
IESWG0001	BLMC-20122-002	68.3	±2.9	68.2	±2.9	66.1	±2.9		
IESWG0002	BLMC-20122-005	29.8	±1.2	29.7	±3.5	28.28	±0.67		
IESWG0003	BLMC-20122-011	34.4	±1.2	34.75	±0.40	34.36	±0.73		
IESWG0004	CAVE-02399-002	184.2	±7.8	184.0	±7.9	184.9	±7.4	185	±47
IESWG0005	CAVE-02399-003	13.08	±0.29	13.22	±0.98	14.3	±2.4		
IESWG0006	CAVE-02399-004	34.82	±0.38	34.78	±0.22	34.76	±0.34		
IESWG0007	CAVE-02399-006	44.6	±1.6	47.9	±1.9	44.6	±3.9		
IESWG0008	CAVE-02399-007	77.2	±1.2	80.4	±4.5	76.9	±1.5		
IESWG0009	CAVE-02399-008	9.23	±0.36	9.19	±0.55	9.45	±0.14		
IESWG000A	CAVE-02399-009	62.4	±2.8	63.9	±1.4	61.73	±0.56		
IESWG000B	CAVE-02399-011	36.1	±2.1	37.29	±0.13	36.46	±0.51		
IESWG000C	CC-001	2.13	±0.24	1.95	±0.27	2.0	±6.8		
IESWG000D	GUMO-00549-001	33.21	±0.70	35.6	±8.0	33.5	±1.4		
IESWG000E	GUMO-00549-002	28.1	±1.6	28.0	±1.6	27.5	±1.6		
IESWG000F	GUMO-00549-003	27.6	±1.3	28.01	±0.31	27.9	±1.7		
IESWG000G	GUPA-00001-001	16.11	±0.43	17.04	±0.55	15.8	±1.0		
IESWG000H	USFS-11290-002	35.69	±0.67	35.90	±0.91	35.76	±0.30		
IESWG000I	USFS-11290-006	53.57	±0.42	54.90	±0.46	53.58	±0.79		
IESWG000J	USFS-11290-007	37.9	±1.8	39.6	±0.4	36.5	±1.7		
IESWG000K	USFS-11290-008	33.5	±2.0	33.08	±0.41	33.06	±0.48		
IESWG000L	USFS-11290-009	54.5	±1.3	56.1	±1.4	55.0	±1.4		
IESWG000M	USFS-11290-010	112.8	0.96	116.4	±1.5	116.8	±1.5	118.8	±0.71
IESWG000N	USFS-11290-011	29.0	±2	27.6	±3.6	26.0	±6.8		

stage attached to a Fluid Inc. Trendicator with a Doric 410A temperature display. The Doric Trendicator 410A was calibrated per the Fluid Inc. instruction manual (Reynolds, 1994). An ice water bath of 18 MΩ H_2O was prepared for the 0°C calibration. The end of the thermistor was submerged in the ice water bath and allowed to equilibrate. Once the temperature stayed constant on the Doric 410A indicator panel, the zero potentiometer was adjusted to 0.0 ± 0.1°C. Liquid nitrogen (LN) was used to freeze a CO_2 standard (standard #1 synthetic fluid inclusion from Syn Flinc) for the low-temperature calibration. Dry N_2 was used to pressurize the liquid nitrogen Dewar. The cold LN flow was set to 14 standard cubic feet per hour (SCFH). After minor adjustment of the span (−) potentiometer, the standard froze at approximately −98°C and melted at −56.6 ± 0.2°C on the final three runs. The zero calibration was checked again in the same manner as above to ensure it had not changed. The high-temperature calibration was run using a Powerstat variable transformer at a setting of 70 to provide heat. Air flow was provided from a compressor set at 15 SCFH. Ten runs were accomplished using the Syn Flinc standard #4 (pure H_2O), with homogenization occurring at 374.1 ± 0.2°C on the final three runs. The zero calibration was checked a final time to ensure that it was still accurate.

2.3.2. Analysis

Each subsample was prepared using a mortar and pestle to gently cleave a thin (100 to 500 μm) piece of crystal selected from the interior of the main sample. This subsample was then surveyed for fluid inclusions with notations made when groups of single phase inclusions were found. Once a two phase inclusion assemblage was located, a photograph was taken and sketch completed of each inclusion or assemblage used for the analysis. Fluid inclusion size was determined by using a Dino-Lite calibration slide to find the pitch of the reticules in the Leica microscope at 500X (40X lens, 12.5X eyepiece) magnification. All heating runs for each sample were repeated a minimum of 3 times, or until the last three runs were within ±1.0°C.

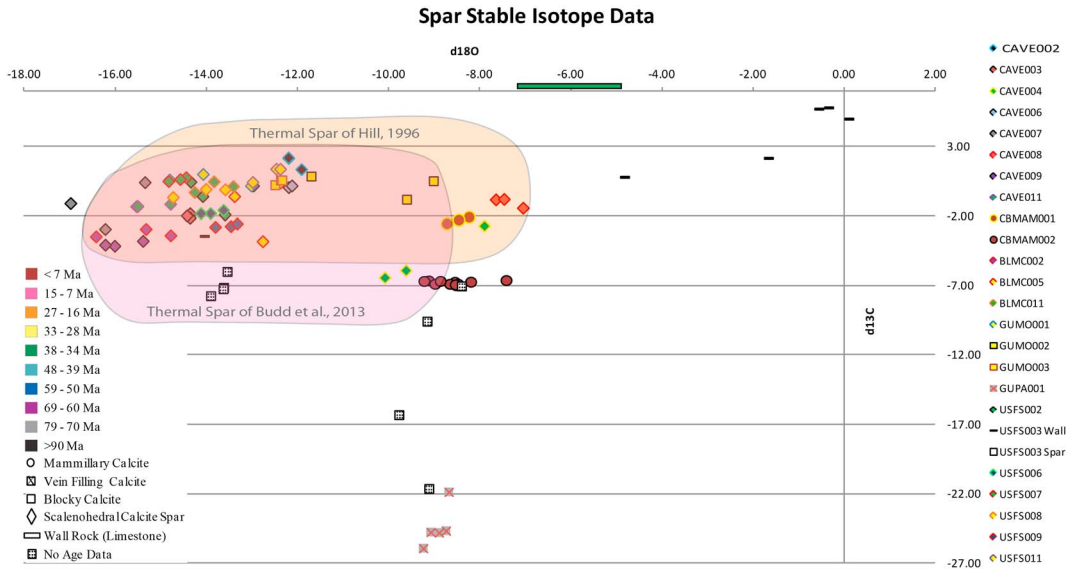

Figure 3. $\delta^{13}C$ versus $\delta^{18}O$. $\delta^{13}C$ values are slightly heavier than would be expected from a magmatic source, indicating possible buoyant hydrothermal mixing with waters in equilibrium with the bedrock. $\delta^{18}O$ values match those of the thermal spar of Hill (1996) and the thermally derived carbonate cements of Loyd et al. (2013) and Budd et al. (2013).

3. Results

3.1. Isotopic Data

3.1.1. U–Pb System

Twenty-two U–Pb-dated cave spar samples (Table 1) from 18 different spar caves located throughout the Guadalupe Mountains (Figure 2) yielded ages between 185 ± 7 and 9.5 ± 0.1 Ma. Greater than 50% of the spar ages are between 36 and 28 Ma, within the period of ignimbrite flare-up (Chapin, Wilks, & McIntosh, 2004). In addition to our cave spar results, fibrous fault-filling calcite sampled from the Border Fault zone in Guadalupe Pass, Texas, yielded an isochron age of 15.8 ± 1.0 Ma that was used as an absolute and direct constraint on the earliest timing of block fault activity, similar to the method used by Roberts and Walker (2016). $^{238}U/^{206}Pb$, $^{235}U/^{207}Pb$, and 3-D concordia ages were all within analytical error (Table 1). Spar ages from two of the caves (Carlsbad Caverns and Lechuguilla Cave) indicate multigenerational spar deposition events within the same cave. For example, Carlsbad Cavern spar had the oldest, 185 Ma, and the youngest, 9 Ma, spar dates. While the spar crystals that yielded these dates are currently located within the same cave, they are from two different spar caves (vugs), separated by nearly a kilometer horizontally, and are only part of the same cave in that younger sulfuric-acid speleogenesis breached both voids and connected them. This is also the case for other vugs within both caves.

3.1.2. Uranium-Series Data

Uranium-series data were monitored during this research to ensure isotopic equilibrium. All samples used in this study have measured values of $^{230}Th/^{238}U$ and $\delta^{234}U$ that indicate that the calcite is in or very near isotopic secular equilibrium, showing that there had been little to no U, Th, and Pb gain or loss, nor any other events that could have "reset the clock," within the timeframe applicable to uranium-series dating.

3.1.3. $^{87}Sr/^{86}Sr$, $\delta^{13}C$, and $\delta^{18}O$

Strontium, carbon, and oxygen isotope data were also collected. Strontium ratios ($^{87}Sr/^{86}Sr$) ranged from 0.708042 in mammillary calcite up to 0.716033 in the cave spar calcite. The $\delta^{13}C_{CaCO3\text{-}VPDB}$ ranged from −24.4 ‰ in the vein spar from Guadalupe Pass up to 1.94 ‰ in the cave spar and the $\delta^{18}O_{CaCO3\text{-}VPDB}$ ranged from −16.2 to −7.4 ‰ (Figure 3 and Table 2).

3.2. Fluid Inclusion Assemblage Data

Fluid inclusion assemblage (FIA) analysis temperatures range from 40 to 80°C (Table 3) with the temperatures of two samples that remain constrained only to above 0°C and below 30°C (based on single phase inclusions that are fluid between 0°C and room temperature and two phase above 30°C). These samples are likely to

Table 2
Strontium, Carbon, and Oxygen Isotopes for Both Spar and Nonspar Calcite

	$^{87}Sr/^{86}Sr$[a]	Abs. err.	$\delta^{18}O_{CaCO3\text{-}VPDB}$	$\delta^{18}O_{H20\text{-}VSMOW}$	$\delta^{13}C_{CaCO3\text{-}VPDB}$	$\delta^{13}C_{CO2}$[b]
BLMC-002A	0.708940	6.43E−05	−15.51	−7.4	−3.24	−6.9
BLMC-002B	0.708940	6.43E−05	−15.51	−8.7	−3.24	−7.9
BLMC-005A1	0.709523	4.28E−05	−12.85	−7.1	−1.30	−6.7
BLMC-005A2	0.709523	4.28E−05	−12.85	−5.6	−1.30	−5.7
BLMC-005D	0.709523	4.28E−05	−12.85	−7.1	−1.30	−6.8
BLMC-011A	0.710446	3.40E−05	−13.84	−8.8	0.14	−5.8
BLMC-011D	0.710446	3.40E−05	−13.84	−8.6	0.14	−5.7
CAVE-002	0.708390	2.50E−04	−12.11	DNA[c]	1.94	NC[c]
CAVE-003A	0.710200	1.10E−03	−14.38	−6.7	−1.94	−5.9
CAVE-003B	0.710200	1.10E−03	−14.38	−5.9	−1.94	−5.3
CAVE-004	0.709787	2.88E−06	−9.21	DNA[c]	−4.98	NC[c]
CAVE-006A	0.710669	6.20E−05	−12.43	−4.8	0.17	−3.9
CAVE-006B	0.710669	6.20E−05	−12.43	−4.9	0.17	−3.9
CAVE-007A	0.708770	5.30E−05	−16.19	−6.3	−1.17	−3.3
CAVE-007B	0.708770	5.30E−05	−16.19	−6.3	−1.17	−3.3
CAVE-008	0.709717	2.02E−06	−7.39	DNA[c]	−0.98	NC[c]
CAVE-009A	0.708695	5.16E−05	−12.34	−3.4	1.18	−1.8
CAVE-009B	0.708695	5.16E−05	−12.34	−3.8	1.18	−2.2
CAVE-011A	0.710483	4.02E−05	−15.28	−6.9	−1.22	−4.6
CAVE-011B	0.710483	4.02E−05	−15.28	−7.6	−1.22	−5.2
GUMO-001A	0.710750	1.19E−04	−13.97	−6.5	0.63	−3.5
GUMO-001B	0.710750	1.19E−04	−13.97	−7.7	0.63	−4.4
GUMO-002	0.712894	8.36E−05	−10.11	DNA[c]	0.22	NC[c]
GUMO-003A	0.712351	2.55E−05	−12.40	−4.8	0.50	−3.6
GUMO-003B	0.712351	2.55E−05	−12.40	−6.8	0.50	−5.1
USFS-002A	0.710875	7.44E−05	−14.10	−11.0	−0.65	−8.0
USFS-002B	0.710875	7.44E−05	−14.10	−5.6	−0.65	−4.0
USFS-006	0.713842	5.80E−05	−13.89	−8.7	−1.70	−7.5
USFS-007	0.712373	2.70E−05	−14.62	−7.6	0.67	−3.8
USFS-008	0.711094	2.63E−05	−14.11	−4.2	−0.24	−2.4
USFS-009A	0.716033	2.70E + 00	−13.53	−3.7	−2.66	−4.8
USFS-009B	0.716033	2.70E + 00	−13.53	−6.9	−2.66	−7.4
USFS-010(W)	0.708653	4.15E−05	DNA[c]	NC[c]	DNA[c]	NC[c]
USFS-010(Y)	0.708272	3.81E−06	DNA[c]	NC[c]	DNA[c]	NC[c]
USFS-011A	0.712901	1.03E−05	−12.60	−7.7	1.10	−5.0
USFS-011B	0.712901	1.03E−05	−12.60	−5.9	1.10	−3.7
Nonspar calcite						
CaCa-BC21-8to12cm	0.708523	1.40E−05	DNA[c]	NC[c]	DNA[c]	NC[c]
CBM-001 (light)	0.708214	9.90E−06	−8.18	DNA[c]	−6.76	NC[c]
CBM-004 (dark)	0.708042	2.80E−05	−8.48	DNA[c]	−2.26	NC[c]
GUPA-00001-001	DNA[c]	DNA[c]	−8.93	DNA[c]	−24.37	NC[c]
LECH VS-1	0.708782	1.30E−05	DNA[c]	NC[c]	DNA[c]	NC[c]
WBC4-Calcite-2006AD	0.708428	2.10E−05	DNA[c]	NC[c]	DNA[c]	NC[c]

[a]Average $^{87}Sr/^{86}Sr$ value for the limestone bedrock 0.707. [b]$\delta^{13}C_{CO2}$ calculated from Romanek et al. (1992): $\varepsilon_{CaCO3\text{-}CO2} = 11.98 - 0.12 * T$ (°C). [c]DNA, data not available; NC, not computed.

have formed between 35° and 40°C and have simply stretched the fluid (Roedder, 1983b) rather than nucleating a vapor bubble. Forced nucleation was attempted by rapidly cooling the sample to 0°C, but nucleation never occurred.

4. Discussion and Conclusion

4.1. Spar Age Temporal Association With Magmatic Activity

The bulk of our U–Pb ages (Table 1) clusters with the $^{40}Ar/^{39}Ar$ ages in the older of two major ignimbrite flare-up subepisodes (Chapin et al., 2004) (Figures 1b and 4) between 36 and 28 Ma. The remainder are coeval with regional igneous events at 45 Ma (Henry, Price, & James, 1991), 55 Ma (Todd, Silberman, & Armstrong, 1975), 65 Ma (Gilmer et al., 2003), 75 Ma (Befus et al., 2008; Breyer et al., 2007), and 90 Ma (Befus et al., 2008), linking

Table 3
Fluid Inclusion Size (Volume Is Estimated Volume of Vapor Phase to Volume of Inclusion), T_h, T_{mi}, and T_{mf}

	Size (units)	Size (μm)	%Volume	T_h (°C)	±	T_{mi} (°C)	±	T_{mf} (°C)	±
BLMC-002A	7	20	11	69.5	1.0	−14.2	0.5	−0.3	0.5
BLMC-002B	10	29	8	61.0	0.5	−21.6	0.5	0.0	0.5
BLMC-005A1	10	29	10	54.3	1.0	N/O	–	−0.2	0.5
BLMC-005A2	5	14	8	63.3	0.5				
BLMC-005D	4	11	5	53.8	0.5	N/O	–	N/O	–
BLMC-011A	3	9	50	50.4	0.5	−3.5	0.5	−1.2	0.5
BLMC-011D	3	9	80	50.7	0.5				
CAVE-003A	25	72	18	66.7	0.5	−1.0	0.5	0.0	0.5
CAVE-003B	15	43	25	71.6	0.5				
CAVE-006A	30	86	10	66.0	0.5	N/O	–	N/O	–
CAVE-006B	45	129	8	65.7	0.5	N/O	–	N/O	–
CAVE-007A	3	9	20	81.9	0.5	−32.1	0.5	−14.2	0.5
CAVE-007B	5	14	15	82.1	0.5				
CAVE-009A	5	14	15	75.2	0.5	−13.6	0.5	−2.0	0.5
CAVE-009B	15	43	15	71.9	0.5	−4.8	0.5	−0.6	0.5
CAVE-011A	80	229	15	71.6	0.5	−4.0	0.5	−0.2	0.5
CAVE-011B	10	29	10	66.5	1.0				
GUMO-001A	15	43	3	65.3	0.5	−9.9	0.5	−0.4	0.5
GUMO-001B	20	57	3	57.6	0.5				
GUMO-003A	20	57	5	65.6	0.7	−5.0	0.5	−1.9	0.5
GUMO-003B	3	9	5	53.2	2.2				
USFS-002A	20	57	9	38.5	0.5	N/O	–	N/O	–
USFS-002B	40	114	20	71.8	0.5	−10.0	1.0	0.0	0.5
USFS-006A	6	17	8	50.9	0.5				
USFS-007A	4	11	8	62.4	0.5	N/O	–	0.0	0.5
USFS-008B	28	80	8	81.8	0.5				
USFS-009A	10	29	8	81.5	0.5				
USFS-009B	2	6	5	59.8	0.5				
USFS-010(Y)A	10	29	10	74.7	0.5	−34.0	0.5	0.0	0.5
USFS-010(Y)C	7	20	8	53.9	0.5				
USFS-010(Y)B	15	43	5	53.6	6.0				
USFS-010(W)ca	50	143	10	58.0	2.0				
USFS-011A	10	29	10	48.8	0.5	−0.2	0.5	1.0	0.5
USFS-011B	10	29	10	59.8	0.5				

Note. N/O, not observed.

them temporally to the igneous episodes associated with Rio Grande rifting (Figures 1b and 4) and other magmatic events, providing evidence that the origin of these caves and the calcite spar that lines them are related to pulses of regional magmatic activity (Figure 1b). The closest surface expression of magmatic activity occurring near the Guadalupe Mountains is within only 11 km of the reef front. These consist of three parallel mafic dikes emplaced during the ignimbrite flare-up (Barker & Pawlewicz, 1987; King, 1948) that continue several kilometers just below the surface to the northeast (intersected by a local potash mine at depth) and likely continue beneath the cliffs of the reef front to the southwest. Our data set also includes younger spar ages at 14.3 ± 2.4 and 9.45 ± 0.14 Ma in Carlsbad Cavern (Table 1). Our two oldest spar ages of 184.9 ± 7.4 and 116.8 ± 1.5 Ma are not coincident with known periods of magmatic activity in the region.

In Figure 1b we break up the locations and ages of reported igneous activity coincident with periods of cave spar formation (also see Figure 4). The nearest Cretaceous rocks (green) in Figure 1b show that this entire region was likely close to sea level as late as the Cretaceous. Using the speleogenesis model from Decker

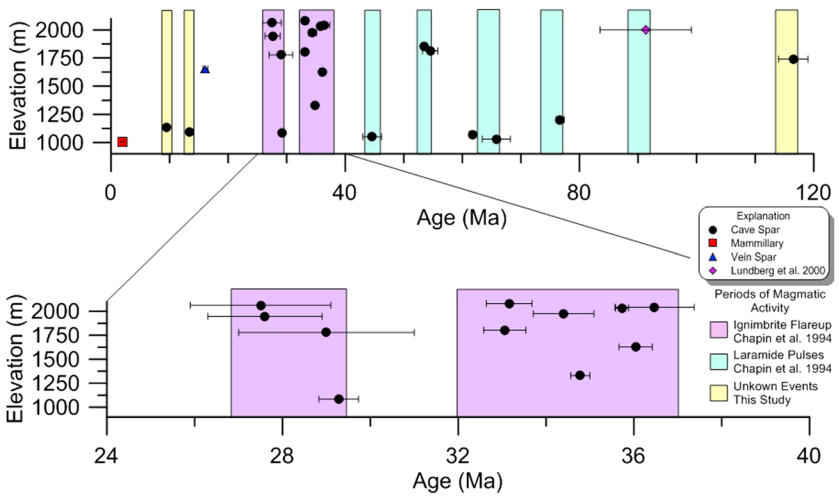

Figure 4. Age versus modern elevation data for cave spar in the Guadalupe Mountains, southeastern New Mexico, and west Texas. Greater than 50% of our age results are within two periods of magmatic activity represented by the ignimbrite flare-up (purple boxes). The light blue bars represent known magmatic activity in the region. The yellow bars are proposed magmatic events based on spar ages, not including a result at 185 Ma. Elevations are used here simply to separate the samples for visual reference and do not represent formation elevations.

et al. (2015), spar dates older than 65 Ma support this evidence for a low-relief, near-sea level landscape. Since then, and up until about 28 Ma, the area was also most likely at or just above sea level. If any significant (>1 km) local rock uplift had occurred, the area where the spar formed would have been lifted out of the spar forming region dropping the water table such that no cave spar could have formed (Figures 5 and 6). Every spar date is an indication of when the spar cave-forming strata were buried to shallow depths of ~0.5 km, and since significant regional uplift would have disturbed the regional water table, it suggests that the surface remained at or near sea level during spar formation.

4.2. Strontium, Carbon, and Oxygen Isotope Interpretation

4.2.1. Strontium

The strontium isotope ratios, ranging from 0.708 to 0.716 (Table 2), are well above that of Late Permian marine limestones (0.7066–0.7084; Hill, 1996; Kani, Hisanabe, & Isozaki, 2013) indicating that the fluid that formed

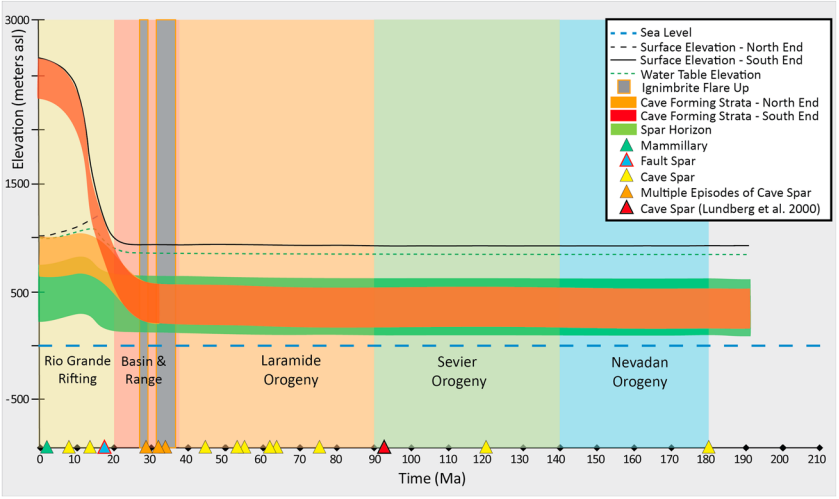

Figure 5. Spar chronology model. Here we show the spar horizon (green ribbon) elevation relative to sea level as far back as the Jurassic period. We also show U–Pb spar ages (yellow, orange, and blue triangles). The red and orange in this graphic represent the southwest and northeast ends of the region of interest, respectively. For example, the southwest end nearest the border fault zone will experience greater uplift than the northeast end near the fault hinges (see Figure 6b).

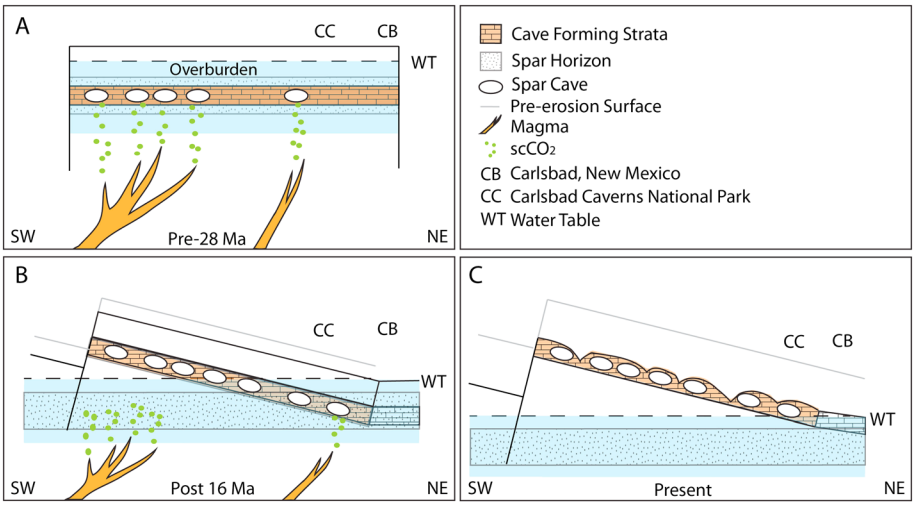

Figure 6. Graphic representation of the formation of the spar caves and spar crystals over time. (a) Volcanism prior to 28 Ma created spar caves and cave spar at the spar horizon ~500 m ± 250 m depth through the release and reaction of supercritical CO_2. (b) As uplift of the Guadalupe block began post-27 Ma, the SW end of the Guadalupe Mountains began to rise and the Capitan Reef was lifted out of the spar horizon to the south as the Guadalupe block began to dewater and erode. To the NE, the spar horizon and cave forming strata remained below the water table. (c) Presently, the Guadalupe Mountains are undergoing erosion and the water table is well below the surface except at the city of Carlsbad where the Capitan Aquifer reaches the surface in the bed of the Pecos River.

the spar was not in complete equilibrium with the Capitan formation or any of the back reef equivalents. This suggests that a component of the groundwater was deeply circulating through, and in contact with, though not in equilibrium with, the basement rock ($^{87}Sr/^{86}Sr$ = 0.82; Barker et al., 1977), which, in this region, is approximately 3.3 km below the surface (Flawn, 1956). One way to explain this is to set up buoyant circulation in a localized hydrothermal plume by heating water at depth and circulating lower Sr ratio waters through higher Sr ratio rocks for a short time (Barker et al., 1977; Shand et al., 2009). Another way is to have a regional aquifer supplied from a distant highland that flows for long periods through high Sr ratio basement rocks. The later seems less likely and would be reflected in more meteoric isotopic signatures of secondary precipitates (Faure & Powell, 1972).

4.2.2. Carbon and Oxygen

The $\delta^{13}C_{spar}$ values for which we have fluid inclusion temperatures range between −3.24 and +1.18 ‰. We estimated the $\delta^{13}C_{CO2}$ of waters forming the calcite assuming equilibrium isotopic fractionation using the measured spar $\delta^{13}C$ values and estimated fluid inclusion temperatures with the enrichment factor equation of Romanek, Brossman, and Morse (1992):

$$\varepsilon_{CaCO3\text{-}CO2} = 11.98\text{–}0.12 * T(°C) \quad (1)$$

Solving for the $\delta^{13}C$ of CO_2 gives a range of −8.0 to −1.8‰, with a mean and standard deviation of −4.9 ± 1.7‰ VPDB (Table 2). These values overlap but are slightly higher than a typical magmatically derived CO_2 signature (−7‰ to −5‰, Figure 3) (El Desouky et al., 2015). The bias toward slightly higher $\delta^{13}C$ values suggests a mix with a high-$\delta^{13}C$ bedrock-derived source. Our observations and estimates are consistent with a locally derived carbon source that is circulating buoyantly, driven by a magmatic heat source, and mixing with meteoric waters.

Similarly, we estimated the $\delta^{18}O$ values of formation water assuming isotopic equilibrium at the estimated spar formation temperatures and the measured $\delta^{18}O$ of spar calcites using the equation of Coplen (2007):

$$1{,}000 \ln \alpha_{calcite\text{-}water} = 17.4(1000/T(°C))\text{–}28.6 \quad (2)$$

and solving for $\delta^{18}O$ of water. The range of the spar $\delta^{18}O$ of −3.4 ‰ to −11.0 ‰ (VPDB) (Table 2) falls directly in line with the thermal spar of Hill (1996) and the thermally derived cements of Loyd et al. (2013) and Budd et al. (2013) (Figure 3). Further, estimated formation water $\delta^{18}O$ values (in Vienna SMOW (VSMOW)) range from −3.4 to −11.0‰, with a mean and standard deviation of −6.6 ± 1.7‰ (Table 2). These values are

Table 4
Vein and Vug Filling Spar Temperatures From McKittrick and Dark Canyons, Guadalupe Mountains, Southeastern New Mexico, and West Texas

Sample	$\delta^{13}C$ (‰ VPDB)	$\delta^{18}O$ (‰ VPDB)	Temp (°C)	Reference
6107-A	−8.4	−11.4	22	1
6107-F	−12.3	−12.8	70	1
6107-I	−12.6	−14.4	74	1
6610-A	−15.4	−15.3	73	1
6610-C	−14.5	−13	71	1
6617-A	−0.6	−15.8	81	1
6617-E	1	−13.9	81	1
6619-A	0.1	−9.9	32	1
6619-C	−1.8	−14	31	1
6626-C	−14.4	−14.9	70	1
6626-E	−16.9	−15.3	75	1
6626-G	−16.8	−15.5	78	1
6626-I	−17.1	−13.6	90	1
6602-A	0.7	−8.8	16	1
6602-D	1	−11.9	65	1
6603-F	−5.4	−12.3	59	1
MC1	1.15	−11.97	72.7	2
MC2	1.16	−11.69	61.6	2
MC3	1.18	−11.6	65.8	2
MC4	1.25	−11.59	63.9	2
MC5	1.34	−11.34	57.8	2
MC6	1.33	−11.41	54.4	2
MC7	1.22	−11.49	58.9	2
MC8	0.53	−8.87	34.8	2
MC9	−5.57	−12.26	40.5	2
MC10	0.86	−11.74	60.1	2
MC11	−1.93	−13.94	50.1	2
MC12	1.18	−11.6	65.8	2
MC13	1.27	−11.82	55.3	2
MC14	−0.81	−14.99	56.5	2
MC15	0.33	−13.77	71.3	2
MC16	0.21	−12.15	67.9	2
MC17	0.82	−11.16	49.7	2
MC18	0.41	−13.23	62.5	2
MC19	−1.38	−16.66	41.2	2
MC20	−0.75	−13.33	55.2	2
DC1	−14.42	−12.88	30.5	2
DC2	−8.12	−11.32	46.7	2
DC3	−17.1	−13.56	58.1	2
DC4	−12.22	−12.65	47.2	2

Note. 1. Budd et al. (2013). Temperatures derived from Δ_{47}. All samples from Dark Canyon. 2. Loyd et al. (2013). Temperatures derived from Δ_{47}. DC, Dark Canyon; MC, McKittrick Canyon.

consistent with a meteoric water source located proximal to an oceanic moisture source relatively unimpeded by significant orographic barriers and are similar to the $\delta^{18}O$ values of summer moisture reaching New Mexico today (Sharp, 2007) and support a mixing of magmatically-derived CO_2 with meteorically derived groundwater.

4.3. Fluid Inclusion Assemblage Interpretation

The fluid inclusion assemblage temperatures of homogenization (40 to 80°C) (Table 3) indicate that the spar formed at temperatures higher than those expected for nonthermal meteoric-derived water, or possibly that the calcite was reset during a postdepositional event. Based on interpretations of the depth of burial after formation of the reef from the study of vitrinite reflectance, petrographic, and isotopic study of syndepositional fracture fills and geomechanical analyses (Barker & Pawlewicz, 1987; Budd et al., 2013; Loyd et al., 2013; Mruk, 1985, 1989; Scholle et al., 1992) (Table 4), the Capitan formation and thus the cave-forming strata were never buried more than about 1 km. Assuming a 20 to 25°C average surface temperature, a local geothermal gradient of between 40 and 60°C/km would have to have been required during the times of spar formation. This strongly suggests geothermal activity and, paired with the timing of formation, magmatically driven geothermal activity. Vitrinite reflectance data from Barker (1987) suggest a regional geotherm of 50°C/km during the ignimbrite flare-up, with steeper gradients likely in areas of hydrothermal upwelling. Present-day geothermal gradients in the region average 25°C/km (Ruppel et al., 2005), supporting our hypothesis that the water from which the cave spar precipitated was thermal. Since the cave spar was formed in vugs where differential pressure is low to nonexistent, and the associated temperatures and pressures of formation were not exceedingly high, it is unlikely that the fluid within the inclusions was reset during higher temperature excursions of events subsequent to the formation of the individual crystals (Roedder, 1983a). Additionally, calcite formation along hydrothermal pathways tends to cement these pathways closed (Budd et al., 2013; Loyd et al., 2013; Mruk, 1985; Scholle et al., 1992), keeping them from being used by later plumes and forcing new pathways to form along unobstructed fractures. This suggests that the T_h for the cave spar in our study is representative of the temperature of formation rather than peak temperatures for the region.

The U–Pb age; $^{87}Sr/^{86}Sr$, $\delta^{18}O$, and $\delta^{13}C$; and data fluid inclusion T_h (Tables 1–3) indicate that the cave spar was formed by mixing of meteoric-derived aquifer water with upwelling deeply circulated meteoric water that was in contact with basement rocks. The calcite formed at elevated temperatures (40 to 80°C) tied to magmatically derived CO_2-related speleogenesis.

4.4. Landscape Evolution of Guadalupe Mountains Region

Two significant findings come from these results: (1) U–Pb ages of cave spar likely define periods of magmatically driven hydrothermal (40 to 80°C) activity responsible for the hypogene speleogenesis (Dublyansky, 2014) of these spar caves, and (2) these ages represent periods when the cave-forming strata were not buried deeper than 1 km below a regional water table (based on our speleogenetic model; Decker et al., 2015), linking age and depth of formation, and therefore can be used to constrain the landscape evolution back into the Cretaceous. These findings are important to any debate regarding the timing and evolution of the rotation of the Guadalupe Mountains tectonic block and the preuplift history of the Delaware Basin region. Our study area is positioned proximally to regional Jurassic rifting (Chihuahua Trough), the Laramide orogeny, Basin

and Range extension, and Rio Grande rifting proper (Figure 1b), allowing for many magmatically driven hydrologic and $scCO_2$ pathways of communication throughout the region, and possibly explaining why our cave spar ages cover the full range of tectono-physiographic history of the region.

Spar ages are sporadic prior to the ignimbrite flare-up but predominantly match the history of magmatic activity in southwestern New Mexico (Chapin et al., 2004) and west Texas (Befus et al., 2008; Breyer et al., 2007; Gilmer et al., 2003; Henry et al., 1991) (Figure 1b). $^{235}U/^{207}Pb$ spar ages at 44.6 ± 3.9, 53.58 ± 0.79, 55.0 ± 1.4, 61.73 ± 0.56, 66.1 ± 2.9, and 76.9 ± 1.5 Ma are coincident within error of individual intrusive dates of regional back-arc magmatism in Trans-Pecos, Texas, and in southwestern New Mexico during the Laramide Orogeny (Befus et al., 2008; Breyer et al., 2007; Chapin et al., 2004; Gilmer et al., 2003; Henry et al., 1991; McLemore, McIntosh, & Pease, 1995). Our interpretation is that these regional-scale magmatic events periodically raised the local thermal gradient and produced copious amounts of CO_2 contributing to the formation of the spar caves and spar linings at ~0.5 km depths. However, our landscape evolution model presented here (Figure 5) suggests that none of these events prior to rifting seemed to result in development of significant topographic relief; otherwise, the area in which the spar caves formed would have been lifted out of the spar horizon during any uplift/down-drop event, precluding the formation of spar younger than the uplift event (Figure 4).

If the surface of the Delaware Basin-Guadalupe Mountains region was moderately (~1 km) uplifted relative to sea level prior to Rio Grande Rift block faulting during the period of interest (185 to 28 Ma), then it would have required a broad epeirogenic uplift to have lifted the regional water table across a large area without changing the gradient drastically, allowing the Capitan reef complex to remain in the spar horizon. Because our U–Pb ages spread between 185 and 28 Ma before Guadalupe block uplift, it seems unlikely that any Laramide or pre-Laramide regional uplift would have been significant (i.e., $>$1 km), which is consistent with broader scale estimates of uplift (Hay, 1984). We interpret the landscape to have been at low elevation (i.e., $<$500 m above sea level) during much of the Jurassic, Cretaceous, and Paleogene (Figure 5) based on our spar forming model (Decker et al., 2015); however, our results and model explained in more detail below allow for broad regional deviations of the landscape elevation of ±500 m band therefore interpretations that place the landscape near sea level during the Cretaceous or near 1,000 m above sea level during the Laramide Orogeny.

We use the age of vein calcite from the Border Fault Zone (BFZ, depicted by the red triangle in Figure 4, GUPA-00001-001, Table 1) to constrain the minimum age of block uplift in the region (Roberts & Walker, 2016). Therefore, between 27 Ma (age of youngest spar near BFZ) and 16 Ma (age of BFZ vein calcite), Rio Grande rift normal faulting and block rotation began lifting the southwestern end of the Guadalupe Mountains tectonic block above and out of the cave spar-forming horizon. The water table at the southwestern end of the mountain range could no longer be supported in the karstic environment and dropped dramatically relative to the strata (Polyak et al., 1998). Considering uplift rates of ~0.11 km/Ma from Polyak, Hill, and Asmerom (2008) and assuming that rate back to initiation of block rotation at 27 Ma or 16 Ma, total uplift along the Border Fault Zone (BFZ) of 2,970 (27 Ma) or 1,760 m (16 Ma) would have occurred, placing the spar horizon between ~0 and 1,000 m above sea level prior to block uplift (Figure 5). This is close to the present-day elevation of the cave-forming strata and water table near the city of Carlsbad. Two postflare-up spar ages at 14.3 ± 2.4 and 9.45 ± 0.14 Ma in Carlsbad Cavern indicate that the northeastern end of the Guadalupe Mountains remained in the spar horizon long after the southwestern end started rising (Figure 6a). It is likely that magmatic events at 14.3 and 9.5 Ma (Seager & Morgan, 1978) coeval with our two youngest spar ages resulted in late spar growth nearer the hinge lines of the Guadalupe block rotation on the southeast end (Figure 6b) that were not yet uplifted. As a result, the areas to the northeast near the hinge line remained well below the water table during the first half of the block uplift period, allowing for continued spar growth after 16 Ma at 14.3 and 9.5 Ma. Eventually, as uplift continued, the water table dropped below even these spar caves and is currently approximately 120 m lower than the lowest known spar caves in the Carlsbad Cavern area. We use the age of a cave mammillary (water table indicator speleothem) from Lake of the Clouds in Carlsbad Cavern (CC001, 2.13 ± 0.24 Ma, Table 1) and the present-day water table to constrain and project the timing of water table descent on the block hinge end of the mountain range.

4.5. Conclusions

We have shown that accurate and precise U–Pb ages can be retrieved from calcite cave spar. Retrieving U–Pb and uranium-series dates from speleothems has been done in the past but has been largely restricted to

stalagmites and other subaerial deposits. Although a spar crystal was dated by Lundberg et al. (2000), this study is the first effort attempting to retrieve radiogenic isotope information from a set of deep phreatic speleothems and, combined with both stable isotope and fluid inclusion data, develop a landscape evolution model from cave spar. We have also shown that the cave spar can be used as a shallow-crust landscape evolution tool based on its deposition in a spar horizon at a known time and a consistent temperature range and depth. Our two oldest spar ages of 185 Ma and 115 Ma in combination with the 91.3 ± 7.8 Ma 3-D concordia age reported by Lundberg et al. (2000), and our results from 77 to 28 Ma, seemingly demonstrate that the study area was at or just above sea level since the Jurassic. On the southwestern end of the mountains in the area of the Border Fault zone along which the Guadalupe Mountains tectonic block was uplifted, two of our results, a cave spar (28 Ma) near the Border Fault zone and fault-filling calcite (16 Ma) in the Border Fault zone, place an absolute constraint on when the block began rising. These results constrain the initiation of uplift of the mountain block to between 28 and 16 Ma. While the Laramide Orogeny is considered as a period of uplift in our study area, there is little known about the extent of Laramide uplift and the pre-Laramide landscape. Some reports suggest that the surface of the region was uplifted as much as 1 km during the Laramide, but the absolute timing of the remaining 2 km of uplift is less well known (Chapin & Cather, 1994; DuChene & Cunningham, 2006; Hill, 1996; Horak, 1985). Overall, our model of spar cave speleogenesis and measured depth results indicate that the paleo-surface of the Guadalupe Mountains and Delaware Basin region was 500 ± 250 m above the spar horizon, and this, along with nearby occurrences of Cretaceous strata (Figure 2) and lack of tectonic evidence for a strong compressional regime during the Laramide, supports a relatively low-lying terrane ~≤1 km above sea level from 180 to 28 Ma, after which the Guadalupe tectonic block rose an additional 2 km above the adjacent salt basin graben on the west end near the fault zone.

The cave spar model, based on the supercritical CO_2 model of spar cave speleogenesis (Decker et al., 2015), proposes that the most likely time spar caves can form is when the cave-forming strata (Capitan Reef, Yates, Tansil, Seven Rivers formations, etc. in our case) intersects the spar horizon (depth at which spar caves and cave spar form). Figure 5 illustrates our proposed model that the landscape in the Guadalupe Mountains remained stable and low-lying during the Cretaceous and through the Laramide and did not begin major uplift until Rio Grande rifting. We demonstrate how cave spar, used as a landscape evolution tool, will augment or compliment AFT analysis and (U-Th)/He data in apatite from regions of igneous and metamorphic provenance as well as provide data in terranes that only have carbonate strata (Farley & Flowers, 2012). The two common shallow crust methods (AHe and AFT) are not useful in our carbonate-dominated study area due to lack of apatite, illustrating the importance of our new method. In areas where data based on shallow crust thermochronometers can be interpreted in more than one way, our newly proposed method of determining landscape evolution could provide the data necessary to resolve the discrepancy.

Acknowledgments
Funding for this research has been provided by the National Science Foundation (NSF; EAR-0214294 and EAR-0518602), the Cave Research Foundation (CRF), the National Speleological Society (NSS), the Cleveland Grotto, the University of New Mexico Alumni Association, and the New Mexico Geological Society (NMGS). We acknowledge facility support from NSF to UNLV to support stable isotopic analyses (EAR-0521196). We would also like to thank Carlsbad Caverns National Park (Dale Pate, Stan Allison and Shawn Thomas), Guadalupe Mountains National Park (Jonena Hearst), Bureau of Land Management, Carlsbad Field Office (Jim Goodbar and Aaron Stockton), and U.S. Forest Service, Guadalupe District (Jason Walz) for their help and support during our field work, and our field assistants, Garrett Jorgensen and Michael Queen. We appreciate access to and use and guidance of the FIA instrument permitted by Jane Selverstone. Discussions with Harvey DuChene helped in our understanding of the fluid flow in the region. All data required for understanding this paper can be found in the graphs, tables, and figures of this paper or in Decker et al. (2015).

References

Austin, G. S. (1978). *Geology and mineral deposits of Ochoan rocks in Delaware Basin and adjacent areas* (88 pp.). Socorro, NM: New Mexico Bureau of Mines and Mineral Resources.

Barker, D. S., Long, L. E., Hoops, G. K., & Hodges, F. N. (1977). Petrology and Rb-Sr isotope geochemistry of intrusions in the Diablo Plateau, northern Trans-Pecos magmatic province, Texas and New Mexico. *Geological Society of America Bulletin*, *88*(10), 1437–1446. https://doi.org/10.1130/0016-7606(1977)88%3C1437:PARIGO%3E2.0.CO;2

Barker, C. E., & Pawlewicz, M. J. (1987). The effects of igneous intrusions and higher heatflow on the thermal maturity of Leonardian and younger rocks, western Delaware Basin, Texas. In D. W. Cromwell, & L. Mazullo (Eds.), *Glass mountains* (pp. 69–83). Society of Economic Paleontologists and Mineralogists.

Befus, K. S., Hanson, R. E., Lehman, T. M., & Griffin, W. R. (2008). Cretaceous basaltic phreatomagmatic volcanism in West Texas: Maar complex at Pena Mountain, Big Bend National Park. *Journal of Volcanology and Geothermal Research*, *173*(3-4), 245–264. https://doi.org/10.1016/j.jvolgeores.2008.01.021

Breyer, J. A., Busbey, A. B., Hanson, R. E., Befus, K. E., Griffin, W. R., Hargrove, U. S., & Bergman, S. C. (2007). Evidence for Late Cretaceous volcanism in Trans-Pecos Texas. *The Journal of Geology*, *115*(2), 243–251. https://doi.org/10.1086/510640

Budd, D. A., Frost, E. L., Huntington, K. W., & Allwardt, P. E. (2013). Syndepostional deformation features in high-relief carbonate platforms: Long-lived conduits for diagenetic fluids. *Journal of Sedimentary Research*, *82*, 12–36.

Chapin, C. E., & Cather, S. (1994). Tectonic settings of the axial basins of the northern and central Rio Grande rift. *Geological Society of America Special Papers*, *291*, 5–26. https://doi.org/10.1130/SPE291-p5

Chapin, C. E., Wilks, M., & McIntosh, W. C. (2004). Space-time patterns of Late Cretaceous to present magmatism in New Mexico—Comparison with Andean volcanism and potential for future volcanism. *New Mexico Bureau of Geology & Mineral Resources*, *160*, 13–40.

Cheng, H., Lawrence Edwards, R., Shen, C. C., Polyak, V. J., Asmerom, Y., Woodhead, J., … Calvin Alexander, E. Jr. (2013). Improvements in 230Th dating, 230Th and 234U half-life values, and U-Th isotopic measurements by multi-collector inductively coupled plasma mass spectrometry. *Earth and Planetary Science Letters*, *371-372*, 82–91. https://doi.org/10.1016/j.epsl.2013.04.006

Chew, D. M., & Spikings, R. A. (2015). Geochronology and thermochronology using apatite: Time and temperature, lower crust to surface. *Elements*, *11*(3), 189–194. https://doi.org/10.2113/gselements.11.3.189

Coplen, T. B. (2007). Calibration of the calcite-water oxygen-isotope geothermometer at Devils Hole, Nevada, a natural laboratory. *Geochemica et Cosmochimica Acta*, *71*(16), 3948–3957. https://doi.org/10.1016/j.gca.2007.05.028

Crysdale, B. L. (1987). Fluid inclusion evidence for the origin, diagenesis and thermal history of sparry calcite cement in the Capitan Limestone, McKittrick Canyon, West Texas (Master of Science thesis) (78 pp.). University of Colorado.

De Muynck, D., Huelga-Auarez, G., Van Heghe, L., Degryse, P., & Vanhaecke, F. (2009). Systematic evaluation of a strontium-specific extraction chromatographic resin for obtaining a purified Sr fraction with quantitative recovery from complex and Ca-rich matrices. *Journal of Analytical Atomic Spectrometry*, *24*(11), 1498–1510. https://doi.org/10.1039/b908645e

Decker, D. D., Polyak, V. J., & Asmerom, Y. (2015). Depth and timing of calcite spar and 'spar cave' genesis: Implications for landscape evolution studies. In J. Feinberg, Y. Gao, & E. C. Alexander, Jr. (Eds.), *Caves and karst across time*, *GSA Special Publication* (Vol. 516, pp. 103–111). Boulder, CO: Geological Society of America.

Denniston, R. F., Asmerom, Y., Polyak, V. J., McNiel, D. F., Klaus, J. S., Cole, P., & Budd, A. F. (2008). Caribbean chronostratigraphy refined with U-Pb dating of a Miocene coral. *Geology*, *36*(2), 151–154. https://doi.org/10.1130/G24280A.1

Donelick, R. A., O'Sullivan, P. B., & Ketcham, R. A. (2005). Apatite-fission track analysis. In P. W. Reiners, & T. A. Ehlers (Eds.), *Low temperature thermochronology: Techniques, interpretations, and applications: Reviews in mineralogy and geochemistry* (Vol. 58, pp. 49–94). Washington, DC: Mineralogical Society of America.

Dublyansky, Y. V. (2014). Hypogene speleogenesis—Discussion of definitions. In A. B. Klimchouk, et al. (Eds.), *Hypogene cave morphologies* (chap. 4.1.5, pp. 158–159). San Salvadore, Bahamas: Karst Waters Institute.

DuChene, H. R., & Cunningham, K. L. (2006). Tectonic influences on speleogenesis in the Guadalupe Mountains, New Mexico and Texas. In L. Land, et al. (Eds.), *New Mexico Geological Society Guidebook, 57th Field Conference, Caves and Karst of southeastern New Mexico* (pp. 211–218). Soccorro, NM: New Mexico Geological Society.

Dumitru, T. A. (2000). Fission-track geochronology. In J. S. Noller, J. M. Sowers, & W. R. Lettis (Eds.), *Quaternary geochronology—Methods and applications* (pp. 131–156). Washington, DC: American Geophysical Union. https://doi.org/10.1029/RF004p0131

Eaton, G. P. (2008). Epeirogeny in the Southern Rocky Mountains region: Evidence and origin. *Geosphere*, *4*(5), 764. https://doi.org/10.1130/GES00149.1

Ehlers, T. A., & Farley, K. A. (2003). Apatite (U-Th)/He thermochronometry: Methods and applications to problems in tectonics and surface processes. *Earth and Planetary Science Letters*, *206*(1-2), 1–14. https://doi.org/10.1016/S0012-821X(02)01069-5

El Desouky, H., Soete, J., Claes, H., & Ozkul, M. (2015). Novel applications of fluid inclusions and isotope geochemistry in unravelling the genesis of fossil travertine systems. *Sedimentology*, *62*(1), 27–56. https://doi.org/10.1111/sed.12137

Farley, K. A. (2002). (U-Th)/He dating: Techniques, calibrations, and applications. In D. Porcelli, C. J. Ballentine, & R. Wieler (Eds.), *Reviews in mineralogy and geochemistry: Noble gases*, (Vol. 47, pp. 819–844). Chantilly, VA: Mineralogical Society of America.

Farley, K. A., & Flowers, R. M. (2012). (U–Th)/Ne and multidomain (U–Th)/He systematics of a hydrothermal hematite from eastern Grand Canyon. *Earth and Planetary Science Letters*, *359–360*, 131–140.

Farley, K. A., & Stockli, D. F. (2002). (U-Th)/He dating of phosphates: Apatite, monazite, and xenotime. In M. J. Kohn, J. Rakovan, & J. M. Huges (Eds.), *Reviews in mineralogy and geochemistry: Phosphates* (pp. 559–577). Chantilly, VA: Mineralogical Society of America.

Faure, G., & Powell, J. L. (1972). *Strontium isotope geology*, (p. 189). New York: Springer. https://doi.org/10.1007/978-3-642-65367-4

Flawn, P. T. (1955). Summary of Southeast New Mexico basement rocks. In *Fifth Field Conference Guidebook* (pp. 114–117). Socorro, New Mexico: New Mexico Geological Society.

Flawn, P. T. (1956). *Basement rocks of Texas and Southeast New Mexico* (261 pp.). Austin: Texas Bureau of Economic Geology, University of Texas.

Flowers, R. M., & Farley, K. A. (2012). Apatite 4He/3He and (U-Th)/He evidence for an ancient Grand Canyon. *Science*, *338*(6114), 1616–1619. https://doi.org/10.1126/science.1229390

Flowers, R. M., & Farley, K. A. (2013). Response to comments on "Apatite 4He/3He and (U-Th)/He evidence for an ancient Grand Canyon". *Science*, *340*(6129), 143. https://doi.org/10.1126/science.1234203

Garber, R. A., Grover, G. A., & Harris, P. M. (1989). Geology of the Capitan Shelf Margin—Subsurface data from the northern Delaware Basin. In P. M. Harris, & G. A. Grover (Eds.), *Subsurface and outcrop examination of the Capitan Shelf Margin, Northern Delaware Basin* (pp. 3–269). San Antonio, TX: Society of Economic Paleontology and Mineralogy. https://doi.org/10.2110/cor.89.13.0003

Gilmer, A. K., Kyle, J. R., Connelly, J. N., Mathur, R. D., & Henry, C. D. (2003). Extension of Laramide magmatism in southwestern North America into Trans-Pecos Texas. *Geology*, *31*(5), 447–450. https://doi.org/10.1130/0091-7613(2003)031%3C0447:EOLMIS%3E2.0.CO;2

Green, P. F., Crowhurst, P. V., Duddy, I. R., Japsan, P., & Holford, S. P. (2006). Conflicting (U-Th)-He and fission track ages in apatite—Enhanced retention, not anomalous annealing behavior. *Earth and Planetary Science Letters*, *250*(3-4), 407–427. https://doi.org/10.1016/j.epsl.2006.08.022

Hay, W. W. (1984). *The breakup of Pangaea, climatic, erosional and sedimentological effects*. Paper Presented at Geology of Ocean Basins. Moscow, Russia: VNU Science Press.

Hayes, P. T. (1964). *Geology of the Guadalupe Mountains, New Mexico* (69 pp.). Washington, DC: U.S. Dep. of the Interior, U.S. Gov. Print. Off.

Hayes, P. T., & Adams, J. E. (1962). *Permian of the Central Guadalupe Mountains, Eddy County, New Mexico* (116 pp.). West Texas and Carlsbad, NM: Roswell and Hobbs Geological Societies.

Hendricks, B. W. H., & Redfield, T. F. (2005). Apatite fission track and (U-Th)/He data from Fennoscandia: An example of underestimation of fission track annealing in apatite. *Earth and Planetary Science Letters*, *236*(1-2), 443–458. https://doi.org/10.1016/j.epsl.2005.05.027

Hendricks, B. W. H., & Redfield, T. F. (2006). Reply to: Comment on "Apatite fission track and (U–Th)/He data from Fennoscandia: An example of underestimation of fission track annealing in apatite" by B. W. H. Hendriks and T. F. Redfield. *Earth and Planetary Science Letters*, *248*(1-2), 569–577. https://doi.org/10.1016/j.epsl.2006.06.022

Henry, C. D., Price, J. G., & James, E. W. (1991). Mid-Cenozoic stress evolution and magmatism in the Southern Cordillera, Texas and Mexico: Transition from continental arc to intraplate extension. *Journal of Geophysical Research*, *96*(B8), 13,545–13,560. https://doi.org/10.1029/91JB00202

Hill, C. A. (1987). *Geology of Carlsbad Cavern and other caves in the Guadalupe Mountains, New Mexico and Texas* (150 pp.). Socorro, NM: New Mexico Bureau of Mines and Mineral Resources.

Hill, C. A. (1993). Sulfide/barite/fluorite mineral deposits, Guadalupe Mountains, New Mexico and west Texas, New Mexico. *Geology*, *15*(3), 56–71.

Hill, C. A. (1996). *Geology of the Delaware Basin, Guadalupe, Apache and Glass Mountains, New Mexico and West Texas* (480 pp.). Albuquerque, NM: Permian Basin Seciton - SEPM.

Hills, J. M. (1984). Sedimentation, tectonism, and hydrocarbon generation in Delaware Basin, West Texas and southeastern New Mexico. *The American Association of Petroleum Geologists Bulletin*, *68*(3), 250–267.

Horak, R. L. (1985). Tectonic and hydrocarbon maturation history in the Permian Basin. *Oil and Gas Journal*, *83*(21), 124–129.
Kani, T., Hisanabe, C., & Isozaki, Y. (2013). The Capitanian (Permian) minimum of 87Sr/86Sr ratio in the mid-Panthalassan paleo-atoll carbonates and its demise by the deglaciation and continental doming. *Gondwana Research*, *24*(1), 212–221. https://doi.org/10.1016/j.gr.2012.08.025
Karlstrom, K. E., Lee, J. P., Kelley, S. A., Crow, R. S., Crossey, L. J., Young, R. A., … Shuster, D. L. (2014). Formation of the Grand Canyon 5 to 6 million years ago through integration of older palaeocanyons. *Nature Geoscience*, *7*(3), 239–244. https://doi.org/10.1038/ngeo2065
Karlstrom, K. E., Lee, J., Kelley, S., Crow, R., Young, R. A., Lucchitta, I., … Crossey, L. (2013). Comment on "Apatite 4He/3He and (U-Th)/He evidence for an ancient Grand Canyon". *Science*, *340*(6129), 143. https://doi.org/10.1126/science.1233982
Kelley, V. C. (1971). Geology of the Pecos country, southeastern New Mexico. *New Mexico Bureau of Mines and Mineral Resources*, *24*, 78.
King, P. B. (1948). Geology of the southern Guadalupe Mountains, Texas. Rep. 215, United States Department of the Interior, Washington, DC.
Kirkland, D. W. (2014). In L. Land (Ed.), *Role of hydrogen sulfide I the formation of cave and karst phenomena in the Guadalupe Mountains and Western Delaware Basin, New Mexico and Texas*, *Monograph of Speleogenesis in the Guadalupe Mountains* (77 pp.). Carlsbad, NM: National Cave and Karst Research Institute.
Lachniet, M. (2009). Climatic and environmental controls on speleothem oxygen isotope values. *Quaternary Science Reviews*, *28*(5-6), 412–432. https://doi.org/10.1016/j.quascirev.2008.10.021
Larson, S. A., Cederbom, C., Tullborg, E.-L., & Stiberg, J.-P. (2006). Comment on "Apatite fission track and (U-Th)/He data from Fennoscandia: An example of underestimation of fission track annealing in apatite" by Hendricks and Redfield. *Earth and Planetary Science Letters*, *248*(1-2), 561–568. https://doi.org/10.1016/j.epsl.2006.06.018
Loyd, S. J., Dickson, J. A. D., Scholle, P. A., & Tripati, A. K. (2013). Extensive uplift-related and non-fault-controlled spar precipitation in the Permian Capitan formation. *Sedimentary Geology*, *298*, 17–27. https://doi.org/10.1016/j.sedgeo.2013.10.001
Ludwig, K. R. (1993). PBDAT: A computer program for processing Pb-U-Th isotope data, 1.2 ed., 30 pp., U.S. Geological Survey.
Ludwig, K. R. (2000). Users manual for Isoplot/Ex version 2.2: A geochronological toolkit for Microsoft Excel, 2.2 ed., 47 pp., Berkely Geochronolgy Center, Berkely, CA.
Lundberg, J. L., Ford, D. C., & Hill, C. A. (2000). Preliminary U-Pb date on Cave Spar, Big Canyon, Guadalupe Mountains, New Mexico, USA. *Journal of Cave and Karst Studies*, *62*(2), 144–148.
Ma, J., Wei, G., Liu, Y., Ren, Z., Xu, Y., & Yang, Y. (2013). Precise measurement of stable (δ 88/86Sr) and radiogenic (87Sr/86Sr) strontium isotope ratios in geological standard reference materials using MC-ICP-MS. *Chinese Science Bulletin*, 1–8.
McLemore, V. T., McIntosh, W. C., & Pease, T. C. (1995). 40Ar/39Ar age determinations of four plutons associated with mineral deposits in southwestern New Mexico. Rep., 36 pp, New Mexico Tech, Socorro, NM.
Meyer, R. F. (1966). *Geology of the Pennsylvanian and Wolfcampian rocks in Southeast New Mexico*. Socorro, NM: New Mexico Bureau of Mines and Mineral Resources.
Mruk, D. H. (1985). *Cementation and dolomitization of the Capitan limestone (Permian), McKittrick Canyon, West Texas* (155 pp.). Boulder, CO, Denver, CO: University of Colorado.
Mruk, D. H. (1989). Diagenesis of the Capitan limestone, upper Permian, McKittrick Canyon, West Texas. In P. M. Harris & G. A. Glover (Eds.), *Subsurface and outcrop examination of the Capitan Shelf Margin, Northern Delaware Basin* (pp. 387–473). San Antonio, TX: SEPM. https://doi.org/10.2110/cor.89.13.0387
Polyak, V. J., Hill, C. A., & Asmerom, Y. (2008). Age and evolution of the Grand Canyon revealed by U-Pb dating of water table-type speleothems. *Science*, *319*(5868), 1377–1380. https://doi.org/10.1126/science.1151248
Polyak, V. J., McIntosh, W. C., Guven, N., & Provencio, P. (1998). Age and origin of Carlsbad cavern and related caves from 40Ar/39Ar of alunite. *Science*, *279*(5358), 1919–1922. https://doi.org/10.1126/science.279.5358.1919
Reiners, P. W., Ehlers, T. A., & Zeitler, P. K. (2005). Past, present & future of thermochronology. In P. W. Reiners, & T. A. Ehlers (Eds.), *Low-temperature thermochronology: Techniques, interpretations, and applications* (chap. 1, pp. 1–18). Chantilly, VA: Mineralogical Society of America.
Renne, P. R. (2000). K-Ar and 40Ar/39Ar dating. In J. S. Noller, J. M. Sowers, & W. R. Lettis (Eds.), *Quaternary geochronology—Methods and applications* (pp. 77–100). American Geophysical Union, Washington, DC.
Reynolds, T. J. (1994). *Fluid Inc. adapted U.S.G.S. gas-flow heating/freezing system instruction manual* (33 pp.). Denver, CO: Fluid Inc.
Roberts, N. M. W., & Walker, R. J. (2016). U-Pb geochronology of calcite-mineralized faults: Absolute timing of rift-related fault events of the northeast Atlantic margin. *Geology*, *44*(7), 531–534. https://doi.org/10.1130/G37868.1
Roedder, E. (1983a). The origin of inclusions. In E. Roedder (Ed.), *Fluid inclusions* (pp. 11–46). Reston, VA: Mineralogical Society of America.
Roedder, E. (1983b). *Fluid inclusions* (646 pp.). Washington, DC: Mineralogical Society of America.
Romanek, C. S., Brossman, E. L., & Morse, J. W. (1992). Carbon isotopic fractionation in synthetic aragonite and calcite: Effects of temperature and precipitation rate. *Geochemica et Cosmochimica Acta*, *56*(1), 419–430. https://doi.org/10.1016/0016-7037(92)90142-6
Ruppel, S. C., Jones, R. H., Breton, C. L., & Kane, J. A. (2005). Preparation of maps depicting geothermal gradients and Precambrian structure in the Permian BasinRep., Bureau of Economic Geology, Jackson School of Geosciences, University of Texas, Austin, Austin, TX.
Schoene, B., Crowley, J. L., Condon, D. J., Schmitz, M. D., & Bowring, S. A. (2006). Reassessing the uranium decay constants for geochronology using ID-TIMS U-Pb data. *Geochemica et Cosmochimica Acta*, *70*(2), 426–445. https://doi.org/10.1016/j.gca.2005.09.007
Scholle, P. A., Ulmer, D. S., & Melim, L. A. (1992). Late-stage calcites in the Permian Capitan formation and its equivalents, Delaware Basin margin, west Texas and New Mexico: Evidence for replacements of precursor evaporites. *Sedimentology*, *39*(2), 207–234. https://doi.org/10.1111/j.1365-3091.1992.tb01035.x
Seager, W. R., & Morgan, P. (1978). Rio Grande rift in southern New Mexico, west Texas, and northern Chihuahua. *American Geophysical Union Special Publication - Rio Grand Rift: Tectonics and Magmatism*, *14*, 87–106.
Shand, P., Darbyshire, D. P. F., Love, A. J., & Edmunds, W. M. (2009). Sr isotopes in natural waters: Applications to source characterisation and water-rock interaction in contrasting landscapes. *Applied Geochemistry*, *24*(4), 574–586. https://doi.org/10.1016/j.apgeochem.2008.12.011
Sharp, Z. (2007). *Principles of stable isotope geochemistry* (1st ed., 344 pp.). NJ: Pearson Prentice Hall.
Todd, V., Silberman, M., & Armstrong, A. (1975). Geochemistry, petrology, and K-Ar ages of igneous rocks in the central Peloncillo Mountains, Hidalgo County. Paper presented at Soc. Guidebook, 26th Field conf., New Mexico Geol., New Mexico.
Wasserburg, G. J., Wetherill, G. W., Silver, L. T., & Flawn, P. T. (1962). A study of the ages of the Precambrian of Texas. *Journal of Geophysical Research*, *67*(10), 4021–4047. https://doi.org/10.1029/JZ067i010p04021